Calibrating IR optical densities for the Gemini Planet Imager Extreme Adaptive Optics Coronagraph apodizers

Anand Sivaramakrishnan[a,b], Rémi Soummer[c], G. Lawrence Carr[d],
Christophe Dorrer[e], Allen Bolognesi[f],
Neil Zimmerman[a,g], Ben R. Oppenheimer[a], Robin Roberts[a,h], and Alexandra Greenbaum[i]

[a] American Museum of Natural History, 79th Street at CPW, New York, NY 10024, USA
[b] Stony Brook University, Stony Brook NY 11794, USA
[c] Space Telescope Science Institute, 3700 San Martin Drive, Baltimore, MD 21218 USA
[d] National Synchrotron Light Source, Brookhaven National Laboratory, Upton, NY 11973
[e] Aktiwave, 241 Ashley Drive, Rochester, NY 14620 USA
[f] Precision Optical Imaging, 7466 West Henrietta Rd., Rush, NY 14543
[g] Columbia University, 550 West 120th Street, New York, NY 10027 USA
[h] CUNY Graduate Center, 365 5th Ave New York, NY 10016
[i] Rensselaer Polytechnic Institute, 110 Eighth Street, Troy, NY USA 12180

ABSTRACT

High contrast imaging sometimes uses apodized masks in coronagraphs to suppress diffracted starlight from a bright source in order to observe its environs. Continuously graded opacity material and metallic half-tone dots are two possible apodizers fabrication techniques. In the latter approach if dot sizes are comparable to the wavelength of the light, surface plasmon effects can complicate the optical density (OD) vs. superficial dot density relation. OD can also be a complicated function of wavelength. We measured half-tone microdot screens' and continuous materials' transmissions. Our set-up replicated the $f/64$ optical configuration of the Gemini Planet Imager's Apodized Pupil Lyot Coronagraph pupil plane, where we plan to place our pupil plane masks. Our half-tone samples were fabricated with 2, 5, and 10 micron dot sizes, our continuous greyscale was High Energy Electron Beam Sensitive (HEBS) glass (Canyon Materials Inc.). We present optical density (OD) vs. wavelength curves for our half-tone and continuous greyscale samples 1.1 – 2.5 μm wavelength range. Direct measurements of the beam intensity in the far field using a Fourier Transform Infrared Spectrograph on Beamline U4IR at Brookhaven National Laboratory's National Synchrotron Light Source (NSLS) provided transmission spectra of test patches and apodizers. We report the on-axis IR transmission spectra through screens composed of metallic dots that are comparable in size with the wavelength of the light used, over a range of optical densities. We also measured departures from simple theory describing the array of satellite spots created by thin periodic grids in the pupil of the system. Such spots are used for photometry and astrometry in coronagraphic situations. Our results pertain to both ground and space based coronagraphs that use spatially variable attenuation, typically in focal plane or pupil plane masks.

Keywords: half-tone microdot screen optical density calibration, high contrast imaging, apodized pupil Lyot coronagraph, National Synchrotron Light Source, Fourier transform infrared transmission spectroscopy

1. INTRODUCTION

Astronomy is at a new frontier of comparative planetary science. Recent advances in adaptive optics (or AO, which corrects atmospheric disturbances to stellar light in real-time), combined with coronagraphy, a technique for suppressing the diffracted flood of light from a star to search its environs for planetary companions and faint protoplanetary disks, will enable the direct detection of warm young extrasolar Jupter-like planets within 50 parsecs of our Sun. These planets are at least 7 orders of magnitude fainter than their parent stars in the H and K spectral bandpasses (with central wavelengths of 1.65 and 2.1 microns respectively).

Further author information: (Send correspondence to A.S.) A.S.: E-mail: anand@amnh.org, Tel: 1 212 313 7653

Techniques and Instrumentation for Detection of Exoplanets IV, edited by Stuart B. Shaklan, Proc. of SPIE
Vol. 7440, 74401C · © 2009 SPIE · CCC code: 0277-786X/09/$18 · doi: 10.1117/12.826955

The Gemini Planet Imager (GPI), a near-IR 'extreme AO' (ExAO) coronagraphic instrument being developed for the twin 8 m Gemini telescopes, is due for first light on the sky in early 2011. With an advanced AO system operating at 2kHz, and 1500 channels of wavefront sensing and correction over an 8 m primary mirror, it is designed to provide a sufficiently flat stellar wavefront to a coronagraph to enable the requisite coronagraphic suppression demanded by these science goals.

Such extreme adaptive optics coronagraphy dedicated to imaging extrasolar planets and disks sometimes uses pupil apodization as a technique to attain high contrast images.[1–4] Pupil plane apodizers can be made by depositing metallic dots on a good optical quality glass substrate in a quasi-random pattern, or by dint of inducing a continously variable opacity in the glass or on its surface. We investigated two apodization technologies: High Energy Electron Beam Sensitive (HEBS) glass (Canyon Materials Inc.), and square metallic dots on glass.

Half-tone screens have also been studied for the ESO-SPHERE and other projects in some detail.[5–7] However, the GPI coronagraphic instrument requires a factor of ten or so more light suppression than the comparable ESO-SPHERE coronagraph,[8] as their search spaces and detection methods are slightly different.[9]

We measured the optical density of calibration test patches with transmissions as low as 1% (*i.e.*, an on-axis intensity attenuation factor of 0.01). GPI's pupil masks' apodization profiles need to match the design profile to about ∼0.5% or better.

We found continuous opacity material too chromatic for our purposes. We also rediscovered anomalously high transmission of light through wavelength-sized holes in metallic screens (*e.g.,* Refs. 11, 12 and references therein). Increasing the half-tone screen's dot size to 10 μm on a side should enable grey apodizers to be fabricated with the requisite accuracy. Test patches with 5 and especially 2 μm dots exhibited rather complex behaviors, particularly when the microdot screens were laid down in periodic patterns such as a checkerboard, as can occur for a desired 0.5 on-axis far-field transmission.

We also examined the effect of a periodic grid of fine opaque lines in the pupil. This grid gives rise to faint ghost images that provide astrometric and photometric fiducials for a coronagraphic image. In coronagraphic situations the intensity of the central object is suppressed to an unknown degree, and its morphology complicated by transmission through the coronagraph, so such fiducials provide stable calibrators for proper motion and photometric measurements of faint structure in a coronagraphic image.[13, 14]

2. TRANSMISSION SPECTROSCOPY WITH SYNCHROTRON RADIATION

2.1 U4IR NSLS BNL Synchrotron beam line

The UV-Optical electron ring at the National Synchrotron Light Source (NSLS) at Brookhaven National Laboratory (BNL) provides a photometrically and optically stable well-collimated IR light source with a compact point-spread function (PSF). It is powerful enough for accurate measurements, in addition to being understood optically. Experimental paradigms used at the U4IR beamline at NSLS are well-defined, enabling beam intensity fluctuations to be calibrated out to well below our desired transmission measurement accuracy.

The IR synchrotron beam from the NSLS visible and ultraviolet electron storage ring feeds a Bruker 66 Fourier Transform Infrared Spectrograph (FTIRS) equipped with a CaFl beamsplitter, to enable IR measurements. An InGaAs single element external detector is connected is to the FTIRS. The FTIRS enables simultaneous measurement of transmission spectra of a sample placed in its beam. The detector's wavelength range was 1.1 - 2.5 μm. We used a spectral resolution of 100 across the range. Our sample was mounted on a computer-controlled X-Y stage with sub-micron positional repeatability. The experiment was run using a proprietary Bruker stage and FTIRS control macro language (OPUS). Spectral data were translated to ascii files recording wavenumber and throughput at each wavenumber.

2.2 Synchrotron beam calibration

Scans of the sample and reference patches were interspersed to enable the internal scatter of measurements to be kept below ∼ 0.2%. A tradeoff between beam stability and the signal to noise ratio in each spectral scan was explored to find suitable combinations.

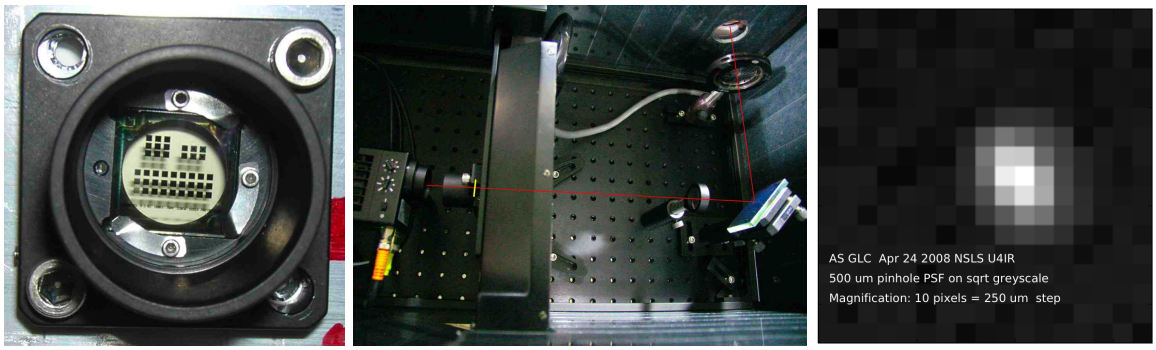

Figure 1. *Left:* Example of a set of calibration patches on a sample, which is mounted in a lens tube. *Middle:* Experimental arrangement. The collimated IR synchrotron beam enters a Bruker 66V Fourier Transform Spectrometer, with its output beam passing through a the circular hole cut in an enclosure. The beam (red line) then passes through an iris diaphragm used to set the desired focal ratio. After reflecting off a fold mirror it is focussed by an IR doublet on the sample mounted on a computer-controlled stage. The sample location is indicated with a small yellow bar drawn transverse to the beam. This stage is the only optomechanical part of the set-up moved during the measurement of a sample. The single-channel InGaAs detector at left in this panel is about 2 mm square. The detector output goes to the FTIR spectrometer. *Right:* PSF of beam on sample measured through a low-quality 500um pinhole at focus (instead of the sample). The spatial step size in this grid is 250 μm. This and other PSF measurements suggest a PSF size of about 200 μm in one direction and 100 μm in the other.

A 3mm iris in front of a 200mm focal length lens selected part of the synchrotron beam (whose cross section is of the order of a few centimeters). The beam position is set by means of fold mirrors with manually adjustable tilts. The beam passing through the iris was focussed to a spot of the order of 200 μm in size (Fig. 1).

Both existing literature and our initial experiments indicated that when the intensity of the beam is attenuated by a factor of 0.5 or more the attenuation becomes an increasingly sensitive function of optical density. Such dependence increases with decreasing dot size. This behavior is not easily calculated either theoretically or numerically. Some one-dimensional models for the expected throughput (given a microdot size and superficial density) exist, but they diverged measurably from our early data at higher optical densities. While this field is under study elsewhere,[11,12] our primary concern was the accurate creation of radially-varying transmission profile of apodizers.[10]

The IR synchrotron beam varies slowly in intensity in-between electron injection into the ring (Fig. 2). Hence reference spectra must be taken at regular intervals to monitor beam stability. The temporal details of measurements has to be optimized enough to achieve required measurement precision given a particular data collection strategy and beam-line behavior. A single spectrum is taken with several scans of a piezo-electrically controlled mirror in the FTIRS. A larger number of scans per spectrum, the longer the data takes to collect. This increases measurement errors due to slow intensity fluctuations of the beam.

A full raster scan of 40 OD calibration patches, together with calibration scans through glass and air, takes on the order of a day. Beam stability itself varies in unpredictable ways, depending on the stability of electron ring. Beamline maintenance can change the beam characteristics enough that calibration of the full set of transmission spectra requires attention to these variations. After calibration, noisy scan rejection, and averaging, our internal accuracy on a transmission spectrum was between 0.1% and 0.3%.

3. APODIZER TECHNOLOGY DOWNSELECTION AND REFINEMENT

We measured transmission spectra of both High Energy Electron Beam Sensitive (HEBS) glass calibration patches and 2 μm metallic dot half-tone screen calibration patches in order to help select between apodizer writing technologies (Figs. 3 and 4). The chromaticity exhibited by the HEBS glass patches led us to focus on the metallic dot technology.

Transmission spectra of the 2 μm dot test patches still shows significant chromaticity in the wavelength range of interest. We then fabricated 5 and 10 μm dot sizes, and measured their transmission spectra. The larger

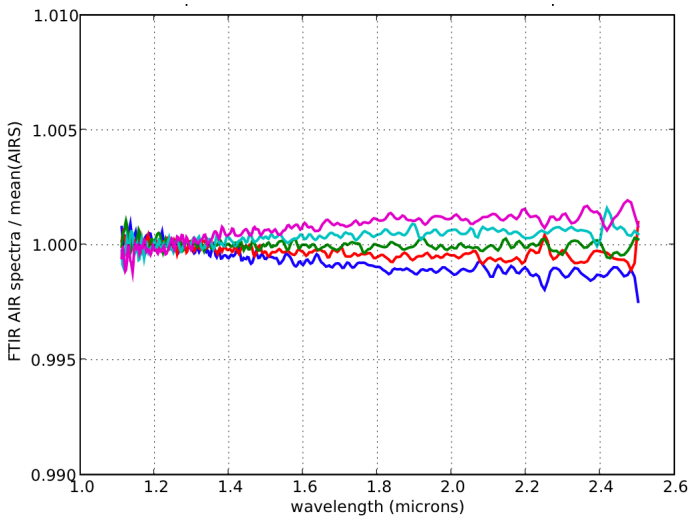

Figure 2. Five sequential spectra through air relative to the mean of all five spectra. Temporal variations like these must be calibrated out by taking reference spectra at appropriate intervals. Such calibration does not work well across fills of the electron ring, which occur about 4 to 5 times in 24 hours.

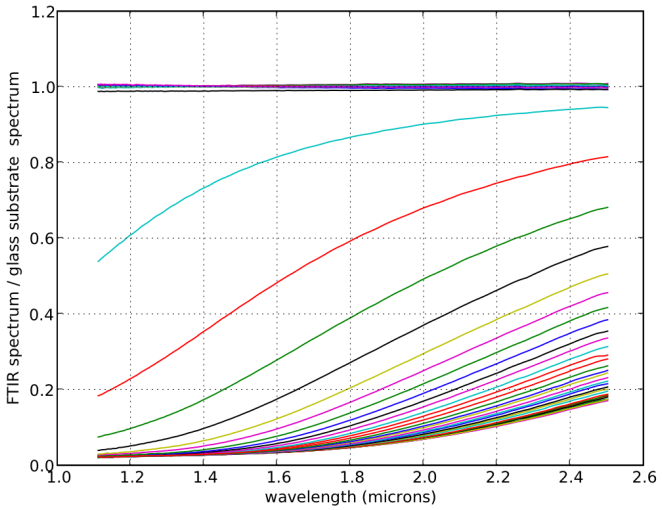

Figure 3. Spectra of a continuous opacity material on Infrasil substrate. The opacity can be a strong function of wavelength, possibly because the opacity is confined to a superficial layer on the glass.

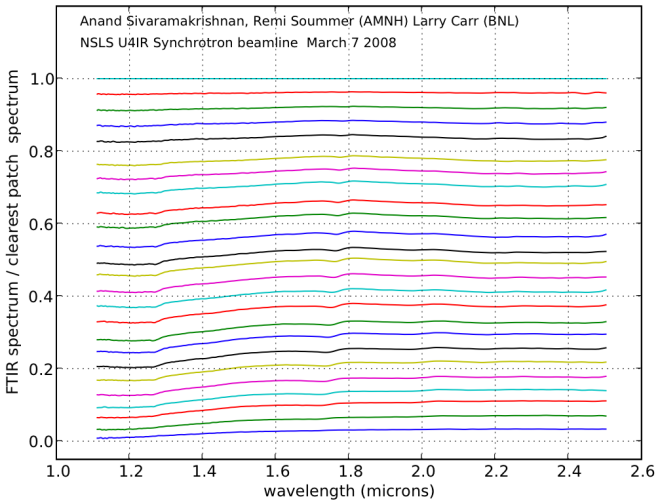

Figure 4. Spectra of uniform optical density (OD) calibration patches fabricated with 2 μm metallic microdots. Chromaticity is far less than for the continuous opacity material, but is still visible from the fact that the curves are not horizontal.

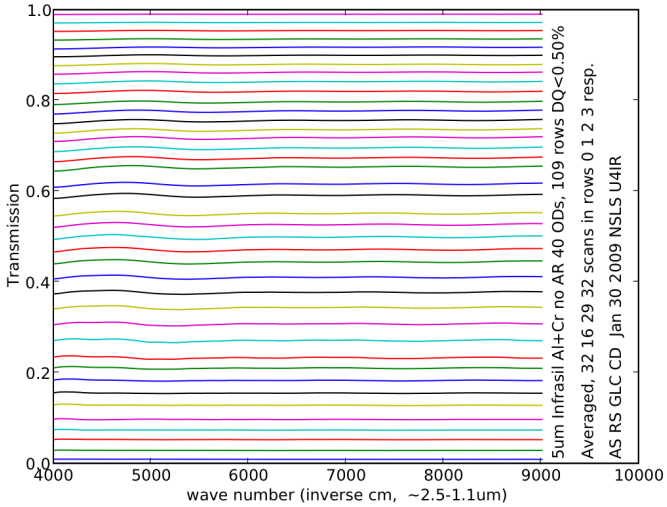

Figure 5. Spectra of uniform optical density (OD) calibration patches fabricated with 5 μm metallic microdots.

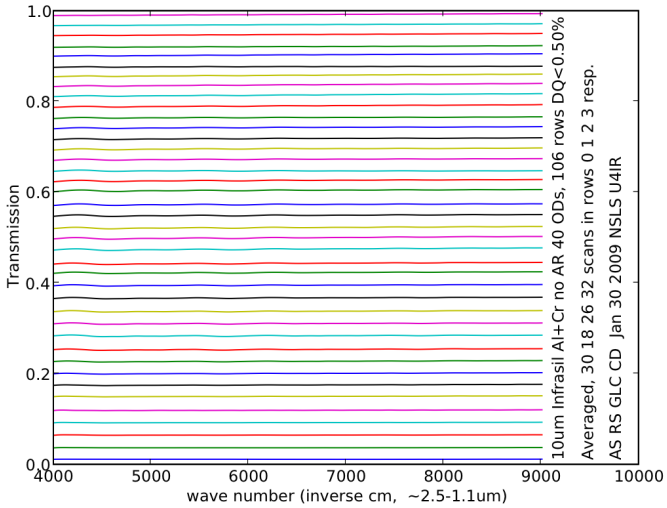

Figure 6. Spectra of uniform optical density (OD) calibration patches fabricated with 10 μm metallic microdots.

the dot sizes displayed far less chromaticity (Fig. 5, 6, 7, 8). Our final selection was the 10 μm dot size for our apodizers.

4. OPACITY MEASUREMENTS AT 1.053 μm WITH AN FPA

As a cross-check we also reimaged an apodizer onto a Focal Plane Array (FPA) detector using 1.053 μm light. In order to measure far field transmission we used a spatial filter in an intermediate image plane. This reproduces the condition of a faster beam than GPI's passing through the apodizer, but it provided a useful cross-reference. Differences between this re-imaging measurement and the BNL NSLS U4IR measurement at the same wavelength is of the order of one to a few percent. However, FPA data is not as easily calibrated as FTIRS data, and the differences in effective focal ratios of the two experimental set-ups suggest that this difference might be understood in terms of detector calibration and diffraction theory.

Radial profiles of a 5 and a 10 μm dot apodizer taken with the FPA are shown in Fig. 9. Transmission accuracy is within our 0.5% requirements except where the transmisions are of the order of 0.25. This far-field transmission occurs when, locally, half of the area is covered with opaque dots and half of the glass is clear. This can be achieved with a checkerboard pattern of opaque dots. As is seen in this figure, anomalouly high transmission occurs in this case. The transmission error is also maximized at a transmission of 0.5 if there is a slight but consistent error in dot size. This is borne out by the IR synchrotron measurements as well, where the desired opacity and measured opacity deviate most when the intensity attenuation is 50%.

5. MICRODOT SIZE EFFECTS ON ASTROMETRIC AND PHOTOMETRIC FIDUCIALS

5.1 Astrometric and photometric fiducial satellite spots

In order to perform astrometry and photometry on coronagraphic images that cannot image the bright primary star along with faint nearby structure or companions in the same exposure, schemes of creating satellite spots by placing a fine grid over a pupil plane have been devised and tested on laboratory testbeds.[13,14] Fig. 10 shows such spots, and the pupil-plane grid written directly on the apodizer.

For GPI our desired satellite spot brightnesses are of the order of 10 astronomical magnitudes fainter than the central star's image in the absence of an occulting coronagraphic focal plane mask. Simple Fraunhofer theory was used to select a grid thickness. We measured the grid-generated satellite spots at 1.65 μm on the GPI

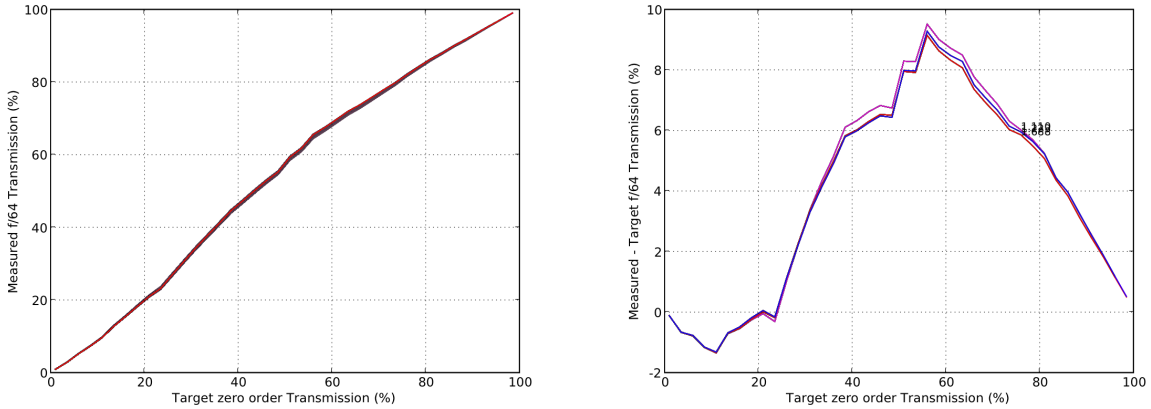

Figure 7. 5 μm microdot patch transmission accuracy for all 40 OD patches: *Left:* target vs. measured *Right*: target vs. measured minus target.

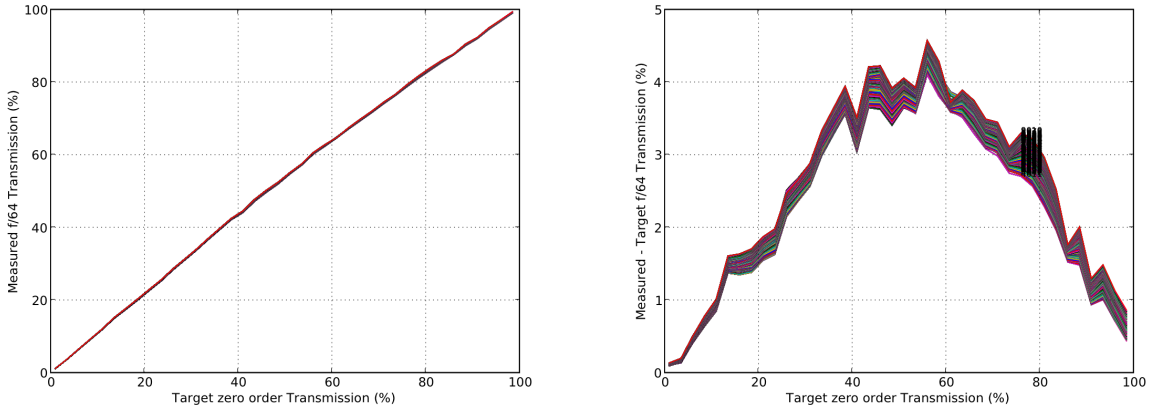

Figure 8. 10 μm microdot patch transmission accuracy for all 40 OD patches: *Left:* target vs. measured *Right*: target vs. measured minus target.

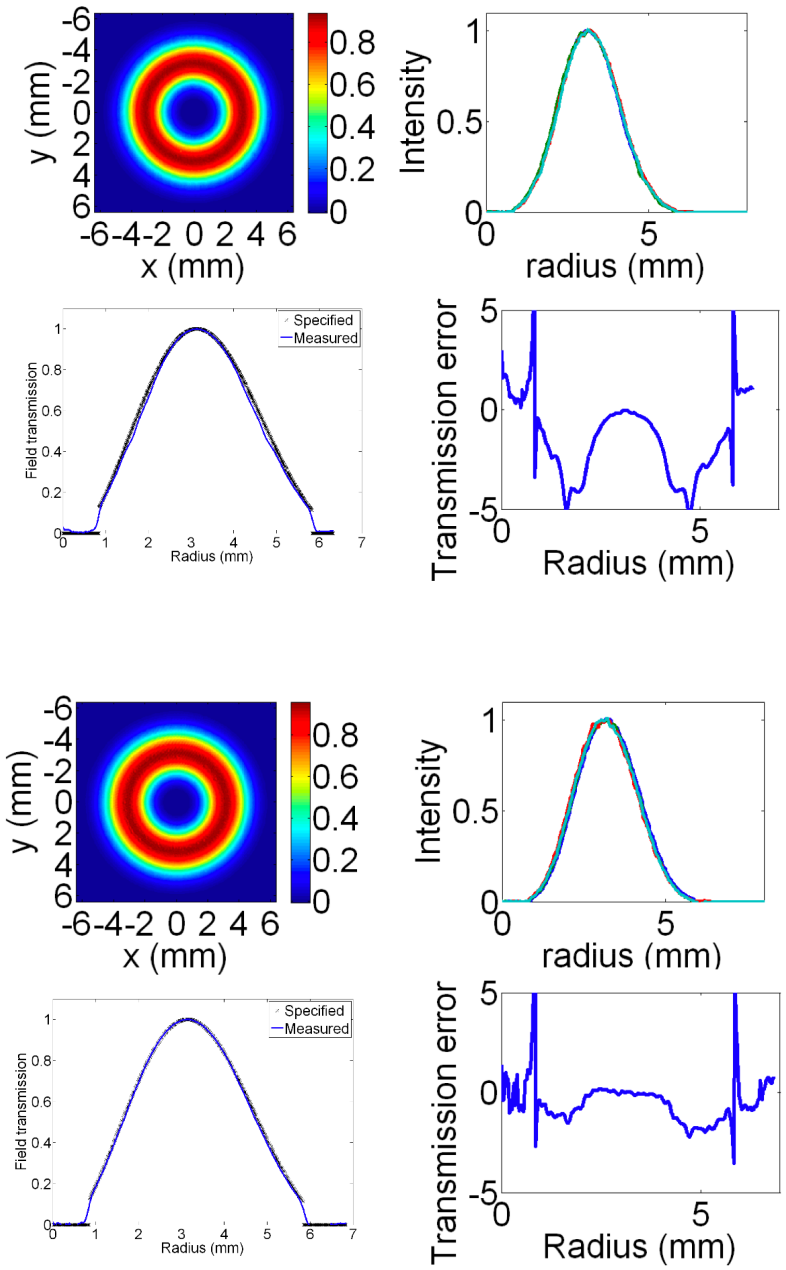

Figure 9. The effect of dot size on expected transmission at 1.053 μm. Apodizers illuminated with collimated light were re-imaged on to a focal plane array detector. The re-imaging optical train incorporated a field stop in order to measure an approximation of the far-field on-axis transmission of the apodizers. *Top:* : Profile of a 5 μm dot apodizer measured at 1.053 μm. The target (specified) and measured profiles as well as the difference between the two is plotted. *Bottom:* The same measurements, performed on the same apodizer design (same target profile), when the apodizer is fabricated with 10 μm dots. These apodizers were written utilizing IR transmission spectra obtained at NSLS, to calibrate the OD vs. dot density relationship. In spite of this "pre-compensation" correction, some difference between the target and measured profiles is detectable. We note that the 10 μm dot profiles exhibit less error than the 5 μm dot ones. In addition, there is a sharp increase in the difference between target and measured OD at a field transmission of 0.5 (or an intensity attenuation of 0.25), where the naive expectation is that a regular checkerboard pattern would produce the desired attenuation.

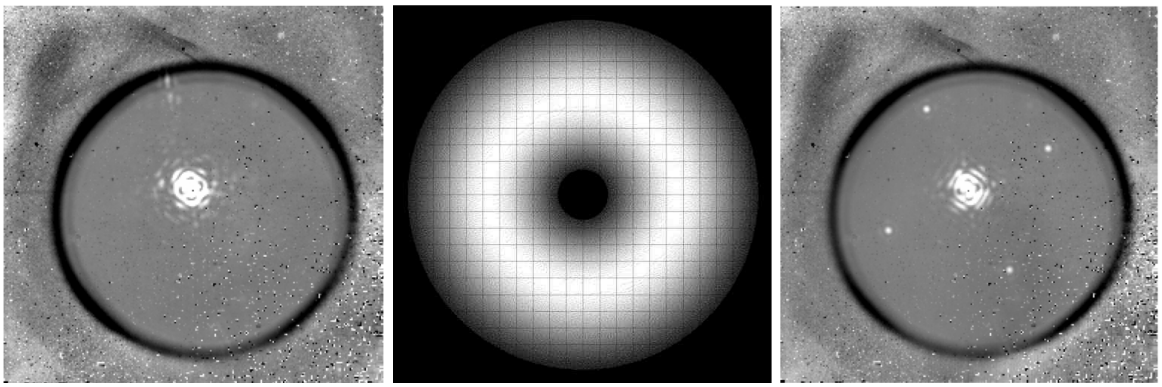

Figure 10. *Left:* A 1.65 μm coronagraphic image used without an astrometric grid in the pupil. *Middle:* Microdot apodizer with an example of a fine opaque grid. *Right:* A 1.65 μm coronagraphic image showing the coronagraphic PSF and the first set of four satellite spots generated by such a grid in the pupil.

Table 1. Astrometric and photometric fiducial satellite image brightness (magnitudes)

Wavelength (μm)	Position	Contrast (mag) (Theory: 10.4)
1.500	8 o'clock	10.93
1.500	2 o'clock	11.05
1.650	8 o'clock	11.10
1.650	2 o'clock	11.18
1.725	8 o'clock	11.17
1.725	8 o'clock	11.17

testbed at AMNH. Table 1 shows that grid lines a few wavelengths in thickness produce fiducial spots are the expected locations, but they are about a magnitude fainter than predictions of simple Fourier optics. With actual measurements at the expected operating wavelength these grid thicknesses can be tailored to suit GPI's performance.

6. CONCLUSION

We selected a microdot-on-glass technology using 10 μm on a side square metallic dots for our 12mm diameter apodizers to be used in the JHK bandpasses on GPI. A requirement on the fineness of the dots relative to the pupil diameter restricts us from using larger dot sizes. Smaller dot sizes, and continuous opacity materials, displayed too much chromaticity in their transmission vs. wavelength behavior. This chromaticity made apodizer design optimization difficult. We also tested the effects of astrometric and photometric grid lines that are on the order of a few wavelengths in width, to produce final apodizer designs for the GPI coronagraph. We also developed experimental paradigms that enabled far-field JHK transmission spectra to be measured to 0.2% or better accuracy, using Brookhaven National Laboratory's National Synchrotron Light Source.

ACKNOWLEDGMENTS

We acknowledge assistance from Dr. Peter Takacs for access to a laminar flow hood at all times of the day, and to Gary Nintzel and Dennis Carlson for rapid, skilled machining of sample mounting hardware. We owe a great debt to Dr. Paul O'Connor of BNL for bringing the NSLS IR beamlines to our attention, thereby enabling us to perform measurements that are essential in order for us to achieve our coronagraphic contrast goals.

REFERENCES

[1] Aime, C., Soummer, R., and Ferrari, A., "Total coronagraphic extinction of rectangular apertures using linear prolate apodizations," *A&A* **389**, 334–344 (2002).

[2] Soummer, R., Aime, C., and Falloon, P. E., "Stellar coronagraphy with prolate apodized circular apertures," *A&A* **397**, 1161–1172 (Jan. 2003).

[3] Soummer, R., "Apodized Pupil Lyot Coronagraphs for Arbitrary Telescope Apertures," *ApJ* **618**, L161–L164 (Jan. 2005).

[4] Sivaramakrishnan, A. and Lloyd, J. P., "Spiders in Lyot Coronagraphs," *ApJ* **633**, 528–533 (Nov. 2005).

[5] Dorrer, C. and Zuegel, J. D., "Design and analysis of binary beam shapers using error diffusion," *Journal of the Optical Society of America B Optical Physics* **24**, 1268–1275 (June 2007).

[6] Martinez, P., Dorrer, C., Aller Carpentier, E., Kasper, M., Boccaletti, A., Dohlen, K., and Yaitskova, N., "Design, analysis, and testing of a microdot apodizer for the Apodized Pupil Lyot Coronagraph," *A&A* **495**, 363–370 (Feb. 2009).

[7] Martinez, P., Dorrer, C., Kasper, M., Boccaletti, A., and Dohlen, K., "Design, analysis, and testing of a microdot apodizer for the apodized pupil Lyot coronagraph. II. Impact of the dot size," *A&A* **500**, 1281–1285 (June 2009).

[8] Beuzit, J.-L., Feldt, M., Dohlen, K., Mouillet, D., Puget, P., Wildi, F., Abe, L., Antichi, J., Baruffolo, A., Baudoz, P., Boccaletti, A., Carbillet, M., Charton, J., Claudi, R., Downing, M., Fabron, C., Feautrier, P., Fedrigo, E., Fusco, T., Gach, J.-L., Gratton, R., Henning, T., Hubin, N., Joos, F., Kasper, M., Langlois, M., Lenzen, R., Moutou, C., Pavlov, A., Petit, C., Pragt, J., Rabou, P., Rigal, F., Roelfsema, R., Rousset, G., Saisse, M., Schmid, H.-M., Stadler, E., Thalmann, C., Turatto, M., Udry, S., Vakili, F., and Waters, R., "SPHERE: a planet finder instrument for the VLT," in [*Society of Photo-Optical Instrumentation Engineers (SPIE) Conference Series*], *Society of Photo-Optical Instrumentation Engineers (SPIE) Conference Series* **7014** (Aug. 2008).

[9] Macintosh, B. A., Graham, J. R., Palmer, D. W., Doyon, R., Dunn, J., Gavel, D. T., Larkin, J., Oppenheimer, B., Saddlemyer, L., Sivaramakrishnan, A., Wallace, J. K., Bauman, B., Erickson, D. A., Marois, C., Poyneer, L. A., and Soummer, R., "The Gemini Planet Imager: from science to design to construction," in [*Society of Photo-Optical Instrumentation Engineers (SPIE) Conference Series*], *Society of Photo-Optical Instrumentation Engineers (SPIE) Conference Series* **7015** (July 2008).

[10] Soummer, R., Sivaramakrishnan, A., Oppenheimer, B. R., Carlotti, A., Pueyo, L., Macintosh, B. A., Bauman, B., Saddlemeyer, L., Erickson, D., Dorrer, C., Caputa, K., Marois, C., Wallace, J. K., Griffiths, E., Mey, J. L., and Kern, B. D. "The Gemini Planet Imager coronagraph testbed," in [*Society of Photo-Optical Instrumentation Engineers (SPIE) Conference Series*], *Society of Photo-Optical Instrumentation Engineers (SPIE) Conference Series* **7440** (August 2009).

[11] Ebbesen, T. W., Lezec, H. J., Ghaemi, H. F., Thio, T., and Wolff, P. A., "Extraordinary optical transmission through sub-wavelength hole arrays," *Nature* **391**, 667–669 (Feb. 1998).

[12] Genet, C. and Ebbesen, T. W., "Light in tiny holes," *Nature* **445**, 39–46 (2007).

[13] Sivaramakrishnan, A. and Oppenheimer, B. R., "Astrometry and Photometry with Coronagraphs," *ApJ* **647**, 620–629 (Aug. 2006).

[14] Marois, C., Lafrenière, D., Macintosh, B., and Doyon, R., "Accurate Astrometry and Photometry of Saturated and Coronagraphic Point Spread Functions," *ApJ* **647**, 612–619 (Aug. 2006).